First-Principles Study on the Origin of the Different Selectivities for Methanol Steam Reforming on Cu(111) and Pd(111)

Xiang-Kui Gu and Wei-Xue Li*

State Key Laboratory of Catalysis and Center for Theoretical and Computational Chemistry, Dalian Institute of Chemical Physics, Chinese Academy of Sciences, Dalian 116023, China

Received: August 13, 2010; Revised Manuscript Received: October 13, 2010

Methanol steam reforming (MSR) is an important industrial process for hydrogen production, and fundamental understanding of the reaction mechanism is crucial to improve the catalytic activity and selectivity. In the present work, we present a comparative mechanistic study of the MSR reaction on two key model systems, Cu(111) and Pd(111), with distinct selectivity using density functional theory calculations. We find that, on Cu(111), methanol dehydrogenation to formaldehyde is favorable first through the O−H bond scission, and the final products are dominated by carbon dioxide and hydrogen. On Pd(111), formaldehyde is also found to be an important intermediate; however, it comes through the C−H bond breaking first, and the final products are mainly CO and hydrogen. We find that the distinct selectivity on the Cu(111) and Pd(111) surfaces originates from the different reactivities of HCHO on the two surfaces. On Cu(111), HCHO tends to react with the hydroxyl to form hydroxymethoxy followed by its decomposition to CO_2. In contrast, direct dehydrogenation of HCHO to CO is favorable on Pd(111). Finally, we find that there is a good linear correlation between the transition-state energies and the final-state energies for the elementary reactions involved in the MSR reaction, which may be useful for computational design and optimization of the catalysts.

1. Introduction

In the past decade, considerable attention has been focused on hydrogen production from hydrocarbons in providing fuel for proton-exchange membrane fuel cell (PEMFC) applications.[1] Although pure hydrogen is a superior feed for PEMFCs, the handling and the storage of hydrogen raise prominent mechanical and safety problems among others.[2,3] In this regard, development of a technology for on-board hydrogen production from liquid hydrocarbons in a microreformer is desirable. Among the liquid hydrocarbons, methanol is considered as a promising alternative because of its high hydrogen to carbon ratio, no carbon−carbon bond, and easy storage and handling requirements.[4,5] Hydrogen production from methanol can be performed by three different catalytic processes, including methanol decomposition (eq 1), methanol steam reforming (eq 2), and partial oxidation of methanol (eq 3).

$$CH_3OH \rightarrow 2H_2 + CO \qquad \Delta H^\circ = 91\ \text{kJ/mol} \qquad (1)$$

$$CH_3OH + H_2O \rightarrow 3H_2 + CO_2 \qquad \Delta H^\circ = 50\ \text{kJ/mol} \qquad (2)$$

$$CH_3OH + {}^1/_2O_2 \rightarrow 2H_2 + CO_2 \qquad \Delta H^\circ = -192\ \text{kJ/mol} \qquad (3)$$

Methanol decomposition is a strongly endothermic reaction producing a large amount of CO, which makes it unsuitable for on-board fuel cell applications as Pt-based anodes are poisoned by CO with a concentration as low as 10 ppm.[6] Therefore, CO must be transferred to CO_2 through the water gas shift reaction.[7−13] Partial oxidation of methanol is an exothermic process with a rapid start-up,[14] but formation of hot spots in the reactor may give rise to sintering of the catalysts.[3] In addition, the corresponding hydrogen yield is lower compared with those of methanol decomposition and methanol steam reforming (MSR). The MSR reaction is a less endothermic reaction providing the highest yield of hydrogen and maintaining high CO_2 selectivity and low CO selectivity.[15] Moreover, the trace CO produced could be removed by preferential oxidation of CO (PROX) with oxygen.[16−18] In this respect, the MSR reaction is more favorable for affording H_2 used in fuel cell applications.

So far, a number of papers have been published on the MSR reaction over the $Cu/ZnO/Al_2O_3$ catalyst[5,19−30] and ZrO_2- and/or CeO_2-promoted Cu-based catalysts,[4,31−35] because of their high activity and selectivity at lower temperatures (200−300 °C). It has been generally agreed that the active component on the Cu-based catalysts for various reactions, including methanol synthesis, decomposition, and steam reforming, is metallic copper.[15] Nevertheless, copper has some significant drawbacks, such as sintering, deactivation, and pyrophoricity. For this reason, many groups have developed active and selective catalysts of group VIII metals. Among them, Pd/ZnO catalysts reported first by Takezawa et al.[36] received particular attention,[36−40] in which the PdZn alloy was suggested as the active phase.

Despite the numerous investigations on the MSR reaction,[5,19,21,27,36,41−44] controversy remains on the reaction mechanism due to the complexity of the reaction. So far, three mechanisms have been proposed and are described as follows:[27]

(A) Methanol decomposition followed by the water gas shift reaction:

* To whom correspondence should be addressed. E-mail: wxli@dicp.ac.cn.

10.1021/jp107678d © 2010 American Chemical Society
Published on Web 11/18/2010

$$CH_3OH \rightarrow CO + 2H_2 \quad (4)$$

$$CO + H_2O \rightarrow CO_2 + H_2 \quad (5)$$

(B) Mechanism via methyl formate:

$$2CH_3OH \rightarrow HCOOCH_3 + 2H_2 \quad (6)$$

$$HCOOCH_3 + H_2O \rightarrow CH_3OH + HCOOH \quad (7)$$

$$HCOOH \rightarrow CO_2 + H_2 \quad (8)$$

(C) Mechanism via formaldehyde:

$$CH_3OH \rightarrow HCHO + H_2 \quad (9)$$

$$HCHO + H_2O \rightarrow HCOOH + H_2 \quad (10)$$

$$HCOOH \rightarrow CO_2 + H_2 \quad (11)$$

Although Peppley et al.[20,21] found that methanol decomposition is much slower than the MSR, they argued that mechanism A should be included over the $Cu/ZnO/Al_2O_3$ catalyst, as the rate of the water gas shift reaction plays an important role in determining the rate of CO formation during the MSR reaction. On the other hand, on the basis of a detailed microkinetic model, Jiang et al.[19] suggested that mechanism A is not applicable on Cu-based catalysts, because the CO yield is less than that predicted from the equilibrium rate constant. They proposed therefore that mechanisms B and C are the main reaction routes, which were supported by Takezawa et al.[36] Despite the differences among the three mechanisms in the MSR reaction proposed, it was agreed in general that the dehydrogenation of surface methoxy groups is the rate-determining step over Cu-based catalysts.

Besides the activity of the MSR reaction, the selectivity is crucial too, and extensive efforts have been done to improve the selectivity, correspondingly. Experimentally, remarkable different selectivities of the MSR reaction over supported copper and group VIII metals has been reported.[36] It was found that supported copper exhibits high selectivity and almost completely transforms methanol to CO_2 and H_2. However, the supported group VIII metal catalysts have lower CO_2 selectivity and convert methanol mainly to CO and H_2. The different catalytic functions of copper and the group VIII metals were attributed to the different reactivities of the HCHO intermediate formed in the MSR reaction over the two catalysts.

Theoretically, to best of our knowledge, a detailed mechanistic study on the activity and selectivity of the whole MSR reaction on Cu and Pd and the origin of their different selectivities are not available yet. So far, most studies have been focused on methanol decomposition, for instance, on Cu(111),[45] Cu(110),[46] Pt(111),[47,48] and Pd(111).[49,50] Recently, Bo et al.[51] investigated the steaming reforming of formaldehyde on the Cu(100) surface using density functional theory (DFT) calculations. To shed light on the activity and selectivity of the overall MSR reaction mechanisms including both the energetics and kinetics of the elementary reactions, we present here a detailed DFT study of the MSR reaction on Cu(111) and Pd(111) surfaces. As the first step, we focus herein on the elementary study on the reaction between the intermediates from methanol decomposition (such as HCHO, HCO, and CO, etc.) and water. The remaining paper is organized as follows. In section 2, the theoretical calculation methods are introduced. In sections 3 and 4, we report the optimized structures and adsorption energies of various intermediates and elementary reactions including reaction energies and reaction barriers involved in the MSR reaction, respectively. A brief discussion of their implication on MSR mechanisms A and C mentioned above is given in section 5. Finally, a brief summary is given in section 6.

2. Theoretical Calculations

Self-consistent periodic DFT calculations were performed using the Vienna ab initio Simulation Package (VASP).[52,53] The interaction between ionic cores and electrons was described by the projector-augmented wave (PAW) method,[54] and the exchange-correlation energy was calculated within the generalized gradient approximation (GGA)[55] and Perdew−Wang 1991 (PW91) functional.[56] The Kohn−Sham equations were solved by using a plane-wave basis set with a kinetic energy cutoff of 400 eV.

All calculations were performed on a periodic 3×3 unit cell comprising nine atoms in each layer, which corresponds to an adsorbate surface coverage of 1/9 of a monolayer (ML). A $5 \times 5 \times 1$ Monkhorst−Pack k-point grid[57] was used to sample the surface Brillouin zone accordingly. The Cu(111) and Pd(111) surfaces were modeled with a four-layer slab model with a 12 Å vacuum between any two successive metal slabs. During the optimization, the atoms in the top two metal layers and adsorbates were allowed to relax using the conjugate-gradient algorithm until the force on each ion was less than 0.05 eV/Å, while the bottom two metal layers were fixed at their bulk positions. (Our test calculations showed that when a more stringent convergence criterion on forces, for instance, 0.001 eV/Å instead of 0.05 eV/Å, was applied, the change in the CO adsorption energy was only 1 meV and therefore was negligible in this particular system.) Adsorption was allowed on only one side of the exposed surfaces, with the dipole moment corrected accordingly in the z direction. Partial occupancies of the wave function were allowed including order-two Methfessel−Paxton smearing[58] with a width of 0.2 eV. All total energies had been extrapolated to zero temperature. The calculated PW91-optimized lattice constants for bulk Cu and bulk Pd were 3.63 and 3.95 Å (in good agreement with the experimental values of 3.62 and 3.89 Å), which were used throughout the present work. The adsorption energies, E_{ads}, were calculated as

$$E_{ads} = E_{ad/sub} - E_{ad} - E_{sub} \quad (12)$$

where $E_{ad/sub}$, E_{ad}, and E_{sub} are the total energies of the optimized adsorbate−substrate system, the adsorbate in the gas phase, and the clean substrate, respectively. The reaction energies, E_r, of the elementary reactions on the substrate were calculated as

$$E_r = \sum (E_{ads})_{products} - \sum (E_{ads})_{reactants} + \Delta E_{gas\ phase} \quad (13)$$

where $\sum(E_{ads})_{products}$ and $\sum(E_{ads})_{reactants}$ are the sums of the adsorption energies of the products and reactants at infinite separation and $\Delta E_{gas\ phase}$ is the corresponding reaction energy in the gas phase. In the definition, positive values of E_{ads} and E_r mean an endothermic and energetically unfavorable process,

TABLE 1: Most Stable Adsorption Sites and Adsorption Energies of the Intermediates Involved in the MSR Reaction on Cu(111) and Pd(111) Surfaces[a]

		adsorption energy (eV)	
intermediate	adsorption site	Cu(111)	Pd(111)
H_2O	top: through O	−0.21	−0.29
CH_3OH	top: through O	−0.17	−0.25
CH_3O	fcc: through O	−2.45	−1.99
CH_2OH	top: through C	−1.11	−1.88
HCHO	O−bridge, C−top	−0.18	−0.64
HCO	C−bridge, O−top	−1.41	−2.51
H_2COOH	O−bridge, O(H)−top	−2.19	−1.88
H_2COO	O−bridge, O−bridge	−4.15	−3.29
HCOOH	O−top, O−H perpendicular to surface	−0.24	−0.42
HCOO	top−bridge−top	−2.92	−2.56
OH	fcc: through O	−3.22	−2.69
CO	fcc: through C	−0.91	−2.12
H	fcc	−2.53	−2.94
CO_2	parallel to surface	−0.05	−0.04

[a] Zero-point energies are not included.

while negative values mean an exothermic and energetically favorable process.

The climbing-image nudged elastic band (CI-NEB) method[59,60] was used to determine the transition states (TSs) for all the elementary reactions. The minimum energy path for each elementary reaction was discretized by a total of eight images between the initial and final states. The TS was denoted by the highest image along the minimum energy path. The activation energy (E_a) of each elementary reaction was calculated by the energy difference between the TS and the initial state. All TSs were confirmed by vibrational frequency analysis, and no zero-point energies were included in the present work.

3. Structures and Energetics of Adsorbed Intermediates

The optimized structures and calculated energetics of various intermediates involved in the MSR reaction on Cu(111) and Pd(111) surfaces, including five saturated molecules (H_2O, CH_3OH, HCHO, HCOOH, and CO) and seven radicals (CH_3O, CH_2OH, HCO, H_2COOH, H_2COO, HCOO, and OH), are discussed in this part. The calculated adsorption energies of the intermediates at the favorable sites are listed in Table 1, and the corresponding configurations are shown in Figure 1.

Water, methanol, and formic acid are bound weakly to the atop sites of the Cu(111) and Pd(111) surfaces through their oxygen atoms (for HCOOH adsorption, the oxygen from HCO− coordinated with the surfaces). The two hydroxyls of adsorbed water are parallel to the surface with O−Cu and O−Pd bond lengths of 2.31 and 2.36 Å, respectively (Figure 1a). The calculated adsorption energies of water are −0.21 eV (Cu) and −0.29 eV (Pd), which agree well with previous DFT results with values of −0.18 eV on Cu(111)[11] and −0.27 eV on Pd(111).[61] The C−O axis of adsorbed methanol is tilted relative to the normal of the substrate by about 57°, and the bond length of O−Cu is 2.29 Å and that of O−Pd is 2.34 Å (Figure 1b). The agreement between the calculated adsorption energies of methanol (−0.17 eV on Cu(111) and −0.25 eV on Pd(111)) and the previous results (Cu(111), −0.16 eV;[45] Pd(111), −0.30 eV[47]) is good. The adsorption energies of *Z*-form formic acid with OH perpendicular to the surface (Figure 1c) are −0.24 eV on Cu(111) and −0.42 eV on Pd(111), which are both more negative (stronger bonding) than those of the adsorbed *E*-form HCOOH by about 0.20 eV (not shown here).

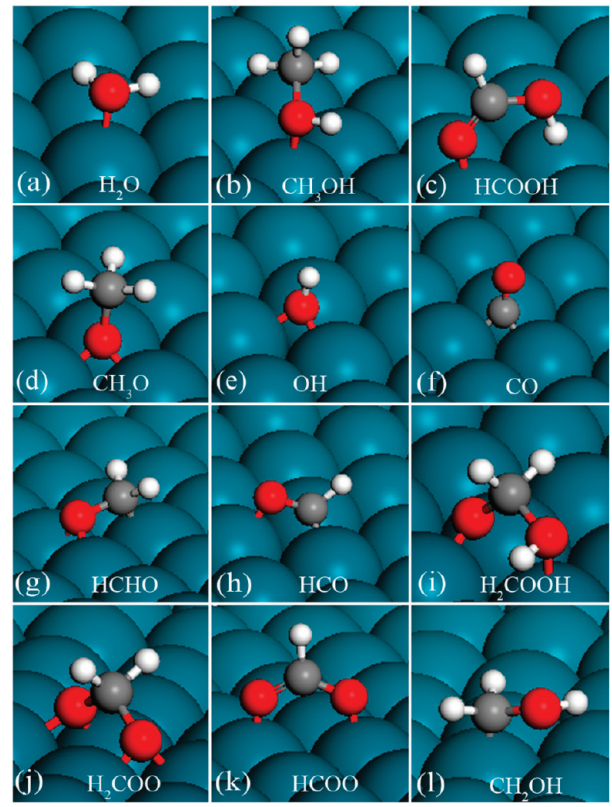

Figure 1. Intermediates involved in the MSR reaction on Cu(111) and Pd(111) at their favorable sites: (a) water, (b) methanol, (c) formic acid, (d) methoxy, (e) hydroxyl, (f) carbon monoxide, (g) formaldehyde, (h) formyl, (i) hydroxymethoxy, (j) dioxymethylene, (k) formate, (l) hydroxymethyl. Labeling of atomic spheres: dark cyan, Cu or Pd; gray, C; red, O; white, H.

Methoxy, hydroxyl, carbon monoxide, and atomic hydrogen prefer to adsorb at the fcc hollow sites of the surfaces. Methoxy and hydroxyl tend to coordinate to the surfaces through their oxygen atoms, while CO tends to coordinate to the surface through its carbon atom (see parts d−f of Figure 1, respectively). The adsorption energies of CH_3O (−2.45 eV) and OH (−3.22 eV) on Cu(111) are more negative than those on Pd(111) (−1.99 and −2.69 eV), whereas the interaction between CO and Cu(111) (−0.91 eV) is weaker than that of CO/Pd(111) (−2.12 eV). The results agree with the previous DFT calculations by Chen et al.,[49] who reported that the adsorption of CH_3O on Cu(111) is stronger than that on Pd(111) by 74 kJ/mol and the adsorption of CO on Cu(111) is weaker than that on Pd(111) by 96 kJ/mol. Atomic hydrogen is energetically favorable to adsorb at the fcc hollow sites, and the calculated adsorption energies are −2.94 and −2.53 eV with respect to atomic hydrogen in the gas phase on Pd(111) and Cu(111), respectively. Compared to water, methanol, and formic acid adsorption studied above, these species have stronger interactions with the two surfaces.

Formaldehyde and formyl prefer top−bridge adsorption on both Cu(111) and Pd(111) surfaces. HCHO forms a top(C)−bridge(O) configuration (namely, C binds to the top site and O to the bridge site, as shown in Figure 1g). The bond strength is modest, and the calculated adsorption energies are −0.18 eV on Cu(111) and −0.64 eV on Pd(111). HCO binds to the surface through O anchoring at an atop site and C sitting at the bridge site and exhibits a top(O)−bridge(C) configuration (Figure 1h), giving a significant bonding of −1.41 eV on Cu(111) and −2.51 eV on Pd(111). Although the configurations of HCHO and HCO

on the two surfaces are similar, the adsorptions of HCHO and HCO on Pd(111) are much stronger than those on Cu(111).

Hydroxymethoxy, dioxymethylene, and formate are prone to anchor on the surfaces by a so-called bidentate structure through their oxygen atoms. H_2COOH with calculated adsorption energies of −2.19 eV on Cu(111) and −1.88 eV on Pd(111) binds to the substrate with the hydroxy oxygen at the top site and the remaining oxygen at the bridge site (Figure 1i). As found in previous work,[62] H_2COO is very active in the gas phase and binds strongly on Cu(111) (−4.15 eV) and Pd(111) (−3.29 eV) surfaces with its two oxygen atoms both at the bridge sites (Figure 1j). HCOO has been studied extensively in the literatures as an important intermediate in the water gas shift reaction on the Cu(111) surface.[11,63] Our calculations are consistent with those results. Namely, HCOO binds strongly to the substrates through two oxygen atoms both sitting at the top sites (Figure 1k) with adsorption energies of −2.92 and −2.56 eV on Cu(111) and on Pd(111), respectively. It is worth noting that the unique geometry of adsorbed HCOO prohibits its further decomposition to CO_2 and H_2, and the corresponding activity is low.

Hydroxymethyl from the C−H bond scission of methanol tends to bind the top site via its carbon atom. The C−O axis is almost parallel to the Cu(111) and Pd(111) surfaces (Figure 1l), and the calculated adsorption energies are −1.11 and −1.88 eV, respectively. As found in HCHO and HCO adsorption, the interaction between CH_2OH and Pd(111) is stronger than that on Cu(111) by 0.77 eV. For carbon dioxide adsorption, the two C−O bonds are parallel to the surfaces, and the bond strengths are rather weak with adsorption energies of −0.05 eV for Cu(111) and −0.04 eV for Pd(111).

Our calculations above show that, for all intermediates considered, corresponding adsorptions on Cu(111) in terms of the site preference and configuration are very similar to those on Pd(111). The saturated molecules except for CO interact weakly with the surfaces, as expected. The strong CO adsorption on the two surfaces comes from its unique donation−back-donation mechanism between CO's $2\pi^*/5\text{-}\sigma$ and the substrate d-band. On the other hand, the radicals bind strongly to the surfaces, which is understandable.

It is interesting to note that, for the intermediates pertinent to the MSR reaction considered, the relative bonding strengths between Cu(111) and Pd(111) present a distinct dependence on the terminal (oxygen and/or carbon) atom of the intermediates coordinated to the surfaces. For O-bound species (such as CH_3O, H_2COOH, H_2COO, HCOO, and OH), the bonding on Cu(111) is stronger than that on Pd(111), whereas for C-bound species (such as CH_2OH, HCHO, HCO, and CO), the bonding on Pd(111) is stronger than that on Cu(111). The difference may come from the significantly strong chemical bond formed between carbon and Pd compared to that of C/Cu, whereas the difference in the oxygen−metal chemical bonds between Cu and Pd is small. Indeed, our DFT calculations find that, for atomic carbon adsorption, the bonding with Pd(111) is 2.00 eV stronger than that of C/Cu(111), whereas the bonding for atomic oxygen with Cu(111) is only 0.25 eV stronger than that of O/Pd(111). In addition, the bonding of atomic hydrogen on Pd(111) is 0.40 eV stronger than that on Cu(111), which indicates that dehydrogenation on Pd is preferential. These differences are essential to the different activities and selectivities for the MSR reaction on Cu(111) and Pd(111) surfaces, as discussed below.

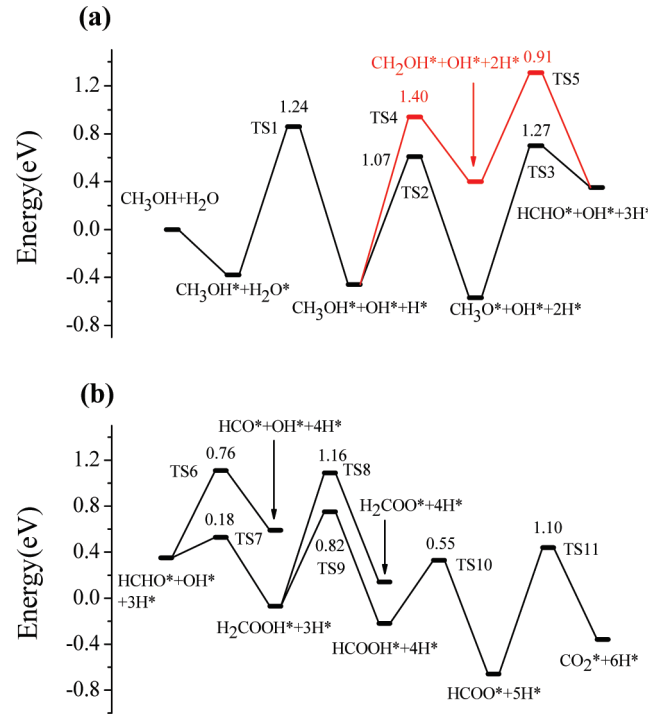

Figure 2. Potential energy surfaces for the MSR reaction on the Cu(111) surface: (a) water dissociation and methanol dehydrogenation to HCHO, (b) HCHO dehydrogenation to HCO and HCHO reaction with OH to form H_2COOH following dehydrogenation to CO_2 and H_2. The zero energy reference is water and methanol in the gas phase plus the clean Cu(111) surface.

4. Activation Barriers and Reaction Energies of Elementary Reactions

We describe here the calculated activation barriers and the reaction energies of key elementary reactions in the MSR reaction, including water dissociation, formation of intermediates from abstraction of hydrogen from methanol, and the sequential reaction with hydroxyl from water. The potential energy surfaces of the overall reaction on Cu(111) and Pd(111) are shown in Figures 2 and 4, respectively. The structures of the corresponding TSs with key bond distances are shown in Figures 3 and 5, and the activation barriers and reaction energies of the elementary reactions are summarized in Table 2.

4.1. Water Dissociation. On the Cu(111) surface, dissociation of adsorbed water to OH and H is nearly thermoneutral with a reaction energy of −0.08 eV, and on the Pd(111) surface it is slightly endothermic with a reaction energy of 0.12 eV. Calculated dissociation barriers are 1.24 and 1.01 eV on the Cu(111) and Pd(111) surfaces, respectively. The present calculations agree well with previous results (1.36 eV for Cu(111) and 1.05 eV for Pd(111)).[11,64] The minimum energy pathway on Cu(111) is that H and OH abstracted from the favorable top-site H_2O move to the two adjacent fcc sites through the TS, where one of the hydroxyls of H_2O is elongated and adsorbs over the bridge site with H and the other OH still sits at the top site (Figure 3, TS1). On Pd(111), a similar result was found (Figure 5, TS1). At the TSs, the bond lengths of the elongated hydroxyls increase by 0.7 Å both for Cu(111) and for Pd(111), compared with those of adsorbed water.

4.2. Methanol Dehydrogenation to HCHO. Two possible pathways for methanol dehydrogenation to HCHO are considered here. For path I, methanol goes first via O−H bond scission to form methoxy followed by further C−H bond scission. For

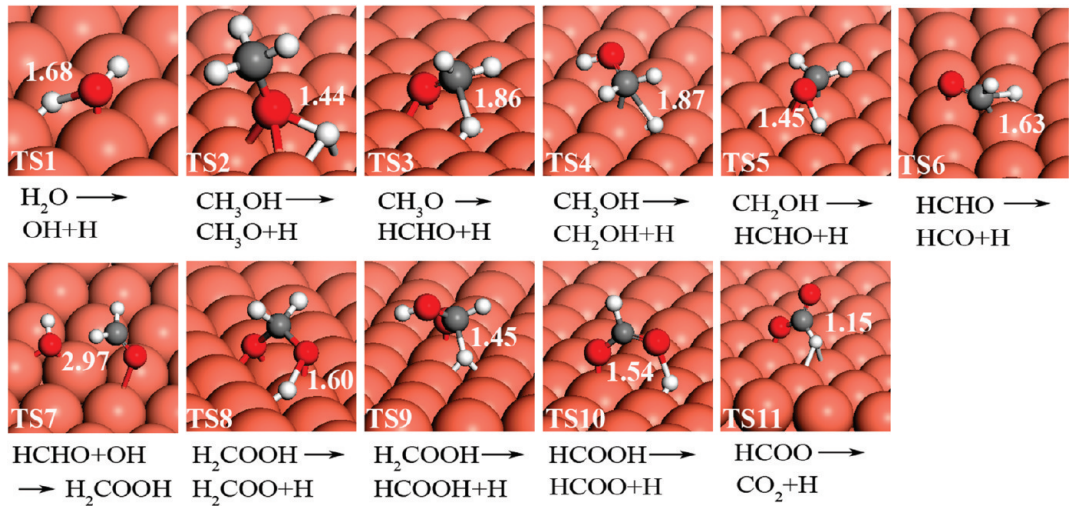

Figure 3. Structures of the optimized transition states (noted in Figure 2) for the MSR reaction on the Cu(111) surface. The numeric values are the key bond distances (Å) for the elementary reactions involved. Labeling of atomic spheres: orange, Cu; gray, C; red, O; white, H.

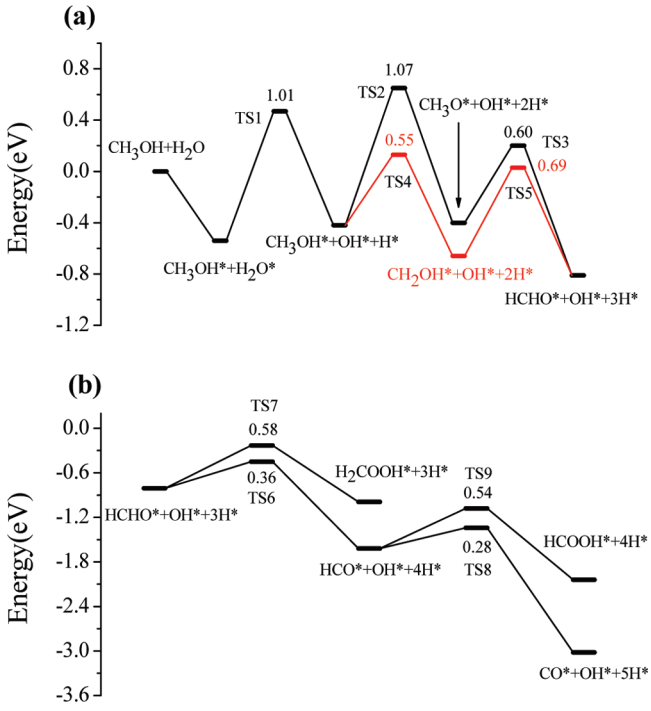

Figure 4. Potential energy surfaces for the MSR reaction on the Pd(111) surface: (a) water dissociation and methanol dehydrogenation to HCHO, (b) HCHO dehydrogenation to CO and HCHO reaction with OH. Energies are relative to gas-phase water and methanol plus the clean Pd(111) surface.

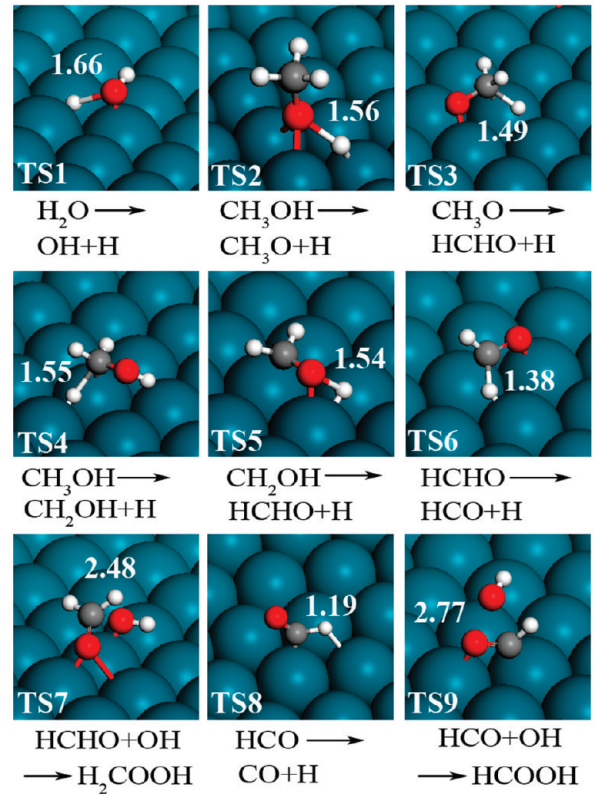

Figure 5. Structures of the optimized transition states (noted in Figure 4) for the MSR reaction on the Pd(111) surface. The numeric values are the key bond distances (Å) for the elementary reactions involved. Labeling of atomic spheres: dark cyan, Pd; gray, C; red, O; white, H.

path II, it goes first through C−H bond scission to form hydroxymethyl followed by sequential O−H bond breaking.

4.2.1. Path I: O−H Bond Scission of Methanol. The O−H bond activation of methanol anchoring at the atop site via oxygen produces the products of CH_3O and H coadsorbed on the adjacent fcc hollow sites. During the O−H bond scission, the CH_3O group moves to the bridge site near the atop site, and the hydroxy hydrogen begins to coordinate with the surface atoms at another adjacent bridge site. At the TSs, the O−H bond length is elongated to 1.44 Å on Cu(111) (Figure 3, TS2) and 1.56 Å on Pd(111) (Figure 5, TS2), compared with 0.98 Å in adsorbed methanol. The hydrogen abstractions of O−H bonds on both Cu(111) and Pd(111) are nearly thermoneutral, and they own an equal energy barrier of 1.07 eV. As found in water dissociation, the activity of O−H scission of methanol would be low due to the weak bonding with the substrates.

4.2.2. Methoxy Dehydrogenation to HCHO. The abstraction of hydrogen from fcc CH_3O, yielding an atomic hydrogen and weakly bound formaldehyde, is strongly endothermic on Cu(111) by 0.92 eV. In contrast, it becomes exothermic on Pd(111) by −0.41 eV. The dramatically different reaction energies on Cu(111) and Pd(111) come from the distinct bonding between reactant/products and the surfaces (see Table 1). Compared to Pd(111), the bonding between CH_3O (reactant) and Cu(111) is 0.46 eV stronger, while the bondings between HCHO and H (products) on Cu(111) are 0.46 and 0.41 eV

TABLE 2: Calculated Activation Barriers (E_a) and Reaction Energies (E_r) for the Elementary Reactions Involved in the MSR Reaction on the Cu(111) and Pd(111) Surfaces[a]

	Cu(111)		Pd(111)	
elementary reaction[b]	E_a	E_r	E_a	E_r
$H_2O^* + * \rightarrow OH^* + H^*$	1.24	−0.08	1.01	0.12
$CH_3OH^* + * \rightarrow CH_3O^* + H^*$	1.07	−0.11	1.07	0.02
$CH_3OH^* + * \rightarrow CH_2OH^* + H^*$	1.40	0.86	0.55	−0.24
$CH_3O^* + * \rightarrow HCHO^* + H^*$	1.27	0.92	0.60	−0.41
$CH_2OH^* + * \rightarrow HCHO^* + H^*$	0.91	−0.05	0.69	−0.15
$HCHO^* + OH^* \rightarrow H_2COOH^*$	0.18	−0.42	0.58	−0.18
$HCHO^* + * \rightarrow HCO^* + H^*$	0.76	0.24	0.36	−0.81
$H_2COOH^* + * \rightarrow H_2COO^* + H^*$	1.16	0.21	*c*	*c*
$H_2COOH^* + * \rightarrow HCOOH^* + H^*$	0.82	−0.15	*c*	*c*
$HCOOH^* + * \rightarrow HCOO^* + H^*$	0.55	−0.44	*c*	*c*
$HCOO^* + * \rightarrow CO_2^* + H^*$	1.10	0.30	*c*	*c*
$HCO^* + OH^* \rightarrow HCOOH^*$	*c*	*c*	0.54	−0.42
$HCO^* + * \rightarrow CO^* + H^*$	*c*	*c*	0.28	−1.40

[a] All values are in electronvolts, and zero-point energies are not included. [b] Asterisks denote the free sites on the Cu(111) and Pd(111) surfaces. [c] Reactions are not considered in this study.

weaker, respectively. This makes the reaction on Cu(111) highly endothermic. During the dehydrogenation, methoxy displaces from the fcc site to the bridge site accompanying the C−O bond axis tilt to facilitate hydrogen abstraction. Corresponding TSs on Cu(111) and Pd(111) are shown in Figure 3 (TS3) and Figure 5 (TS3), respectively. The dehydrogenation barrier of 1.27 eV on Cu(111) is much higher than that of 0.60 eV on Pd(111) accordingly.

4.2.3. Path II: C−H Bond Scission of Methanol. For the C−H bond scission of methanol, corresponding products are hydroxymethyl and H. To approach the TS, the O−C bond tilts toward the surface, and the carbon atom starts to coordinate to the surface metal atoms, facilitating the C−H bond scission. At the TSs (Figure 3, TS4; Figure 5, TS4), the C−H bonds become 1.87 Å on Cu(111) and 1.55 Å on Pd(111), which are significantly elongated compared with that of 1.10 Å in adsorbed methanol. Calculated barriers are 1.40 eV on C(111) and 0.55 eV on Pd(111), and the corresponding reaction energies are 0.86 and −0.24 eV, respectively. It is clear that the low barrier on Pd(111) is driven mainly by the energetics, namely, the stronger bonding between the products (CH_2OH and H) and Pd(111) than that on Cu(111).

4.2.4. O−H Bond Scission of Hydroxymethyl to HCHO. HCHO may also be formed via the O−H bond scission of hydroxymethyl. During this process, the oxygen atom displaces downward to the surface metal atoms to release a H atom while the C atom remains sitting on the top site. At the TSs (Figure 3, TS5; Figure 5, TS5), the distances of O−surface metal atoms are 2.20 Å for Cu(111) and 2.25 Å for Pd(111), while they are 2.21 and 2.61 Å for adsorbed CH_2OH on Cu(111) and on Pd(111), respectively. On Cu(111), the reaction is nearly thermoneutral (−0.05 eV) with a barrier of 0.91 eV, and it becomes slightly exothermic (−0.15 eV) with a barrier of 0.69 eV on Pd(111).

As shown above, there are two possible reaction pathways for methanol dehydrogenation to HCHO. On Cu(111), calculated elementary reaction barriers are 1.07 eV (O−H bond scission of methanol) and 1.27 eV (methoxy dehydrogenation) for path I and 1.40 eV (C−H bond scission of methanol) and 0.97 eV (hydrogen abstraction of CH_2OH) for path II. On Pd(111), the corresponding barriers are 1.07 and 0.60 eV for path I and 0.55 and 0.69 eV for path II. It is clear that, for methanol dehydrogenation to HCHO, path I is preferred on Cu(111) with a maximum elementary barrier of 1.27 eV. On Pd(111), path II is preferred with a maximum elementary barrier of 0.69 eV. The different reaction paths and activities on the two surfaces are driven by the energetics. As shown in Table 1, the CH_3O adsorption energy on Cu(111) is 0.46 eV lower than that on Pd(111), and in contrast, the CH_2OH adsorption energy on Cu(111) is 0.77 eV higher than that on Pd(111). The corresponding reaction energies for methanol dehydrogenation to formaldehyde are endothermic (0.81 eV) via path I on Cu(111) and exothermic (−0.39 eV) via path II on Pd(111). In this context, we note that, for methanol dehydrogenation to formaldehyde, the preference of path I on Cu but path II on Pd found here has also been reported in the literature, for instance, Cu(111),[45] Cu(110),[46] Cu(100),[65] Pd(111),[50] and the Pd cluster.[66] These indicate that methanol dehydrogenation to formaldehyde on Cu and Pd is structure insensitive.

4.3. HCHO Dehydrogenation to HCO and HCHO Reaction with OH. ***4.3.1. HCHO Dehydrogenation to HCO.*** The dehydrogenation of HCHO to HCO is slightly endothermic with a reaction energy of 0.24 eV on Cu(111) and highly exothermic with a reaction energy of −0.84 eV on Pd(111). Calculated barriers are 0.76 and 0.36 eV, respectively. In the literature, Lim and co-workers[67] reported 80 and 38 kJ/mol for this reaction on Cu(111) and Pd(111), which agrees well with the present calculations. Modest dehydrogenation barriers on both surfaces come mainly from their geometries, in which the C−O bond in both the reactant (HCHO) and product (HCO) is parallel to the surface and both C and O atoms are coordinated to the surface atoms. The unique geometries allow the hydrogen abstraction easily without involving a large geometric change. At the TSs (Figure 3, TS6; Figure 5, TS6), the lengths of the cleavage C−H bonds are 1.63 Å on Cu(111) and 1.38 Å on Pd(111), which are 0.53 and 0.27 Å longer than their counterparts in adsorbed HCHO, respectively.

4.3.2. HCHO Reaction with OH. Parallel to HCHO dehydrogenation, HCHO could react with OH from dissociated water to form hydroxymethoxy (H_2COOH). On Cu(111), the calculated reaction barrier is 0.18 eV and the corresponding reaction energy is −0.42 eV. On Pd(111), the corresponding values are 0.58 and −0.18 eV. At the TSs (Figure 3, TS7; Figure 5, TS7), HCHO is lifted up from the substrates to accommodate the attacking hydroxyl. The bonding strength between HCHO and the substrates would affect therefore the corresponding barrier. Indeed, as reported above, HCHO binds 0.46 eV stronger to Pd(111) than to Cu(111), which would result in a higher barrier and less energy gain on Pd(111).

The above results indicate that, on the Cu(111) surface, HCHO tends to react with OH to form H_2COOH ($E_a = 0.18$ eV), instead of dehydrogenate to HCO ($E_a = 0.78$ eV). In contrast, on Pd(111), HCHO tends to dehydrogenate ($E_a = 0.36$ eV) rather than react with OH ($E_a = 0.58$ eV). The barriers for HCHO reaction with OH to form H_2COOH on Cu(111) and HCHO dehydrogenation to HCO on Pd(111) are very low. This means that, though HCHO is an important intermediate for the MSR reaction on both surfaces, it would be difficult to observe experimentally due to its fast kinetics. In the following, we focus therefore only on the reactivity of H_2COOH on Cu(111) and HCO on Pd(111).

4.4. Hydroxymethoxy Dehydrogenation to CO_2 on Cu(111). Hydroxymethoxy dehydrogenation on Cu(111) may proceed first by breaking either the O−H bond or the C−H bond. Our calculations show that the barrier for breaking the O−H bond to form bidentate H_2COO and H (Figure 3, TS8) is considerable with a value of 1.16 eV while the barrier of the C−H bond

scission to form *Z*-form HCOOH and H (Figure 3, TS9) is modest with a value of 0.82 eV. Calculated reaction energies are 0.21 and −0.15 eV, respectively. Since the C−H bond scission of H_2COOH is both energetically and kinetically favorable, only *Z*-form HCOOH dehydrogenation is considered in the following. The *Z*-form HCOOH dehydrogenation to formate (HCOO) is exothermic with a reaction energy of −0.44 eV, and the calculated reaction barrier is 0.55 eV. At the TS (Figure 3, TS10), the O−H bond is elongated by 0.53 Å, and the leaving H adsorbs at the bridgelike site. The product HCOO coordinates to the surface in a bidentate configuration.

In the literature, Mei et al. systematically studied HCOO decomposition on Cu(111) by DFT calculations,[63] suggesting that HCOO dehydrogenation to CO_2 is much faster than its decomposition to HCO. Therefore, we only consider the HCOO dehydrogenation here. The reaction pathway for HCOO dehydrogenation contains two steps. First, the bidentate HCOO transforms to the unidentate isomer by raising the energy by 0.53 eV, which binds to the hollow site with one oxygen atom. Second, the C−H bond of unidentate HCOO is elongated toward the surface for hydrogen abstraction (Figure 3, TS11). The barrier for this process is 0.57 eV, and the produced CO_2 will desorb quickly from the surface. The overall barrier for these processes is 1.10 eV, and the corresponding reaction energy is 0.30 eV. The result is consistent with previous calculations (1.30 eV)[63] and agrees well with available experimental results of 1.10 ± 0.16 eV reported by Nishimura et al.[68]

4.5. HCO Dehydrogenation to CO and HCO Reaction with OH on Pd(111). The C−H bond scission of HCO to form CO and H on Pd(111) is strongly exothermic by −1.40 eV, giving a low barrier of 0.28 eV. The corresponding TS is shown in Figure 5 (TS8). Compared to adsorbed HCO, the C−H bond is only slightly elongated by 0.08 Å, and the TS is initial-state-like. The addition reaction between HCO and OH to form HCOOH is exothermic by −0.42 eV, and the calculated barrier is 0.54 eV. These show clearly that, on Pd(111), HCO prefers to dehydrogenate further to CO and H, instead of react with adsorbed OH to form HCOOH.

5. Discussion

The overall potential energy surfaces including reaction energies and barriers of the elementary reactions for the MSR reaction on Cu(111) and Pd(111) are shown in Figures 2 and 4, respectively. For Cu(111), the main results are as follows: Methanol dehydrogenates first through the O−H bond scission followed by the C−H bond breaking to form HCHO. Second, HCHO reacts with OH from water dissociation to form H_2COOH. Finally, H_2COOH dehydrogenates via the C−H bond scission to form HCOOH, followed by a complete dehydrogenation to CO_2 and H. The rate-determining step is the methoxy dehydrogenation, which agrees well with the experimental results.[19,21,36] The dominant products for MSR reaction on Cu(111) are carbon dioxide and hydrogen.

For Pd(111) (Figure 4), the main products are CO and OH/H from the sequential dehydrogenation of methanol and water dissociation. Different from Cu(111), HCHO comes from the C−H bond scission of methanol first, followed by the O−H bond breaking afterward. The sequential dehydrogenation of HCHO to CO is facile with barriers lower than 0.36 eV. We note that methanol decomposition to CO may proceed via the hydroxymethylene (HCOH) intermediate. This pathway turns out not to be favorable, as reported in the literature on both Pd(111)[50] and the Pd cluster.[66] The activity between CO and OH from water (water gas shift reaction) is low, because a previous DFT calculation showed that palladium is inactive for this reaction.[69] Therefore, the dominant products for the MSR reaction on Pd(111) are carbon monoxide and hydrogen, as found in experiment.[36] This indicates that metallic Pd alone is not a suitable catalyst for methanol steam reforming. Indeed, Pd is often alloyed with another transition metal (for instance Zn) to improve the selectivity.[36−40]

The above calculations show further that there are two differences for the MSR reaction on Cu(111) and that on Pd(111). One is the reaction pathway for the formation of HCHO. On Cu(111), it goes through the O−H bond scission followed by the C−H bond breaking, whereas on Pd(111), the C−H bond scission followed by the O−H bond breaking is favorable. The second difference is the reactivity of HCHO produced. On Cu(111), it prefers to react with OH from dissociative water to form H_2COOH with a small barrier of 0.18 eV, and then H_2COOH decomposes further to CO_2 with an elementary barrier of 1.10 eV at maximum. On Pd(111), however, HCHO tends to dehydrogenate directly to CO and H with a modest barrier of 0.36 eV. The different reactivities of HCHO between Cu(111) and Pd(111) is the reason for the distinct selectivity of the MSR reaction on the two surfaces. Moreover, the present calculations indicate that, for the MSR reaction, mechanism A, namely, methanol decomposition followed by the water gas shift reaction (eqs 4 and 5), would be favorable on Pd(111), while mechanism C via a formaldehyde intermediate (eqs 9−11) would be favorable on Cu(111).

The above calculations show that the distinct reactivity and selectivity for the MSR reaction on Cu(111) and Pd(111) decided by activation energies of the elementary reaction depend sensitively on the energetics of the reactants/products as well as the reaction energies. In the literature, it was found that, for a given elementary reaction, there is a linear scaling relationship between the activation barriers and the reaction energies on different transition-metal surfaces, the so-called Brønsted−Evans−Polanyi (BEP) relation.[70−75] The linear correlation between the activation barriers and the reaction energies from similar transition states has been studied and explored extensively for understanding the catalytic reaction and rationalizing the catalyst design. It would allow estimating the activation energy using adsorption energies of the reactants/products without explicitly optimizing the corresponding transition states, which saves significant computational cost.

For the elementary reactions with rather different transition states on a given transition-metal surface, the linear correlation is not necessarily true. Indeed, there is no linear correlation between calculated activation energies and reaction energies among various elementary reactions considered in the MSR reaction on Cu(111) and Pd(111) here. However, a linear correlation could be found when all the intermediates in the gas phase are used as the zero energy reference, namely, the energies at the transition states, E_{TS}, and the energies of the initial states or the final states, E_{FS} (in the present work), are calculated with respect to the corresponding intermediates in the gas phase. The obtained result for the MSR reaction on Cu(111) and Pd(111) is shown in Figure 6 in detail, and this extended BEP has already been found in various reactions in the literature.[48,66,76,77] However, the origin for this linear correlation remains elusive. We present here a preliminary analysis. When a given intermediate (corresponding counterparts of either reactants or products adsorbed on the surface) in the gas phase approaches the surface, it will be gradually activated by the surface: the closer to the surface, the more activated. The structure at the transition state would typically be less activated

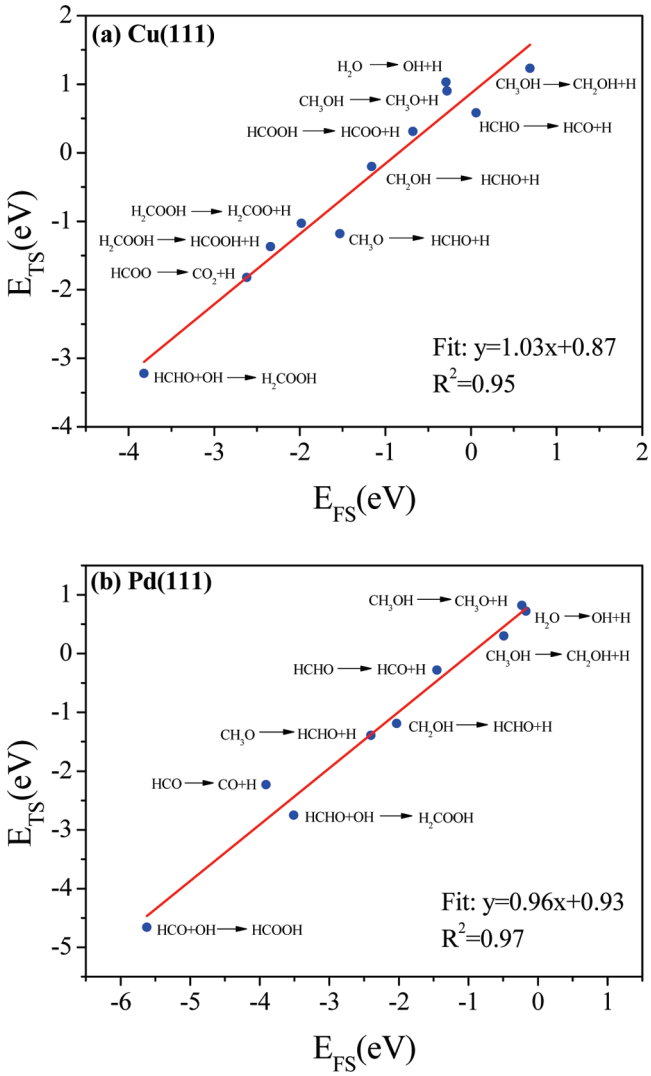

Figure 6. Correlation of the transition-state energies versus the final-state energies for the elementary reactions in the MSR reaction on the Cu(111) and Pd(111) surfaces. The zero energy reference is the corresponding reactants in the gas phase, as noted in the text.

compared to adsorbed reactants/products. On the other hand, we note that for a given catalyst or a transition-metal surface, it has its own intrinsic activity. It is therefore expected that the difference in the activation between the transition states and adsorbed reactants/products on a given transition-metal surface would be less sensitive to the different intermediates, and a linear correlation occurs correspondingly even for the reaction with rather different transition states.

6. Conclusions

Self-consistent density functional calculations are performed to investigate the methanol steam reforming reaction on Cu(111) and Pd(111) in terms of adsorption of various intermediates and elementary reaction energies and barriers, which provide valuable insight into the reaction mechanisms and the origin of the different selectivities on the two surfaces. We find that the adsorption of the C-bound species and H on Pd(111) is stronger than that on Cu(111), while the adsorption of the O-bound species on Cu(111) is stronger than that on Pd(111). The different adsorption properties of these species significantly affect the activity and selectivity of the MSR reaction on the two surfaces.

We find that, on both surfaces, formaldehyde from methanol dehydrogenation via first O−H bond scission on Cu(111) and C−H bond scission on Pd(111) plays an important role in the whole MSR reaction. On Cu(111), formaldehyde produced tends to react with hydroxyl to form hydroxymethoxy, which leads selectively to CO_2 and H. On Pd(111), it tends to a complete dehydrogenation to CO and H. Finally, we find that there is a good linear scaling correlation between the transition-state energies and the final-state energies for the elementary reactions involved in the MSR reaction on Cu(111) and Pd(111), which may be useful for computational design and optimization of catalysts.

Acknowledgment. We thank the Natural Science Foundation of China (Grants 20873142 and 20733008) and Ministry of Science and Technology of China (Grant 2007CB815205) for financial support.

References and Notes

(1) Navarro, R. M.; Pena, M. A.; Fierro, J. L. G. *Chem. Rev.* **2007**, *107*, 3952–3991.
(2) Pettersson, L. J.; Westerholm, R. *Int. J. Hydrogen Energy* **2001**, *26*, 243–264.
(3) Lindstrom, B.; Pettersson, L. J. *Int. J. Hydrogen Energy* **2001**, *26*, 923–933.
(4) Agrell, J.; Birgersson, H.; Boutonnet, M.; Melian-Cabrera, I.; Navarro, R. M.; Fierro, J. L. G. *J. Catal.* **2003**, *219*, 389–403.
(5) Agrell, J.; Birgersson, H.; Boutonnet, M. *J. Power Sources* **2002**, *106*, 249–257.
(6) Acres, G. J. K.; Frost, J. C.; Hards, G. A.; Potter, R. J.; Ralph, T. R.; Thompsett, D.; Burstein, G. T.; Hutchings, G. J. *Catal. Today* **1997**, *38*, 393–400.
(7) Song, C. S. *Catal. Today* **2002**, *77*, 17–49.
(8) Denkwitz, Y.; Karpenko, A.; Plzak, V.; Leppelt, R.; Schumacher, B.; Behm, R. J. *J. Catal.* **2007**, *246*, 74–90.
(9) Rodriguez, J. A.; Ma, S.; Liu, P.; Hrbek, J.; Evans, J.; Perez, M. *Science* **2007**, *318*, 1757–1760.
(10) Si, R.; Flytzani-Stephanopoulos, M. *Angew. Chem., Int. Ed.* **2008**, *47*, 2884–2887.
(11) Gokhale, A. A.; Dumesic, J. A.; Mavrikakis, M. *J. Am. Chem. Soc.* **2008**, *130*, 1402–1414.
(12) Rodriguez, J. A.; Graciani, J.; Evans, J.; Park, J. B.; Yang, F.; Stacchiola, D.; Senanayake, S. D.; Ma, S. G.; Perez, M.; Liu, P.; Sanz, J. F.; Hrbek, J. *Angew. Chem., Int. Ed.* **2009**, *48*, 8047–8050.
(13) Chen, C. S.; Lin, J. H.; Lai, T. W.; Li, B. H. *J. Catal.* **2009**, *263*, 155–166.
(14) de Wild, P. J.; Verhaak, M. *Catal. Today* **2000**, *60*, 3–10.
(15) Palo, D. R.; Dagle, R. A.; Holladay, J. D. *Chem. Rev.* **2007**, *107*, 3992–4021.
(16) Wootsch, A.; Descorme, C.; Duprez, D. *J. Catal.* **2004**, *225*, 259–266.
(17) Alayoglu, S.; Nilekar, A. U.; Mavrikakis, M.; Eichhorn, B. *Nat. Mater.* **2008**, *7*, 333–338.
(18) Fu, Q.; Li, W. X.; Yao, Y. X.; Liu, H. Y.; Su, H. Y.; Ma, D.; Gu, X. K.; Chen, L. M.; Wang, Z.; Zhang, H.; Wang, B.; Bao, X. H. *Science* **2010**, *328*, 1141–1144.
(19) Jiang, C. J.; Trimm, D. L.; Wainwright, M. S.; Cant, N. W. *Appl. Catal., A* **1993**, *93*, 245–255.
(20) Peppley, B. A.; Amphlett, J. C.; Kearns, L. M.; Mann, R. F. *Appl. Catal., A* **1999**, *179*, 21–29.
(21) Peppley, B. A.; Amphlett, J. C.; Kearns, L. M.; Mann, R. F. *Appl. Catal., A* **1999**, *179*, 31–49.
(22) Purnama, H.; Ressler, T.; Jentoft, R. E.; Soerijanto, H.; Schlogl, R.; Schomacker, R. *Appl. Catal., A* **2004**, *259*, 83–94.
(23) Kniep, B. L.; Ressler, T.; Rabis, A.; Girgsdies, F.; Baenitz, M.; Steglich, F.; Schlogl, R. *Angew. Chem., Int. Ed.* **2004**, *43*, 112–115.
(24) Velu, S.; Suzuki, K.; Okazaki, M.; Kapoor, M. P.; Osaki, T.; Ohashi, F. *J. Catal.* **2000**, *194*, 373–384.
(25) Wang, L. C.; Liu, Y. M.; Chen, M.; Cao, Y.; He, H. Y.; Wu, G. S.; Dai, W. L.; Fan, K. N. *J. Catal.* **2007**, *246*, 193–204.
(26) Lin, Y. G.; Hsu, Y. K.; Chen, S. Y.; Lin, Y. K.; Chen, L. C.; Chen, K. H. *Angew. Chem., Int. Ed.* **2009**, *48*, 7586–7590.
(27) Papavasiliou, J.; Avgouropoulos, G.; Ioannides, T. *Appl. Catal., B* **2009**, *88*, 490–496.
(28) Turco, M.; Bagnasco, G.; Costantino, U.; Marmottini, F.; Montanari, T.; Ramis, G.; Busca, G. *J. Catal.* **2004**, *228*, 43–55.

(29) Gunter, M. M.; Ressler, T.; Jentoft, R. E.; Bems, B. *J. Catal.* **2001**, *203*, 133–149.
(30) Matsumura, Y.; Ishibe, H. *J. Catal.* **2009**, *268*, 282–289.
(31) Jones, S. D.; Hagelin-Weaver, H. E. *Appl. Catal., B* **2009**, *90*, 195–204.
(32) Arena, F.; Barbera, K.; Italiano, G.; Bonura, G.; Spadaro, L.; Frusteri, F. *J. Catal.* **2007**, *249*, 185–194.
(33) Huang, G.; Liaw, B. J.; Jhang, C. J.; Chen, Y. Z. *Appl. Catal., A* **2009**, *358*, 7–12.
(34) Matter, P. H.; Braden, D. J.; Ozkan, U. S. *J. Catal.* **2004**, *223*, 340–351.
(35) Udani, P. P. C.; Gunawardana, P.; Lee, H. C.; Kim, D. H. *Int. J. Hydrogen Energy* **2009**, *34*, 7648–7655.
(36) Takezawa, N.; Iwasa, N. *Catal. Today* **1997**, *36*, 45–56.
(37) Chin, Y. H.; Dagle, R.; Hu, J. L.; Dohnalkova, A. C.; Wang, Y. *Catal. Today* **2002**, *77*, 79–88.
(38) Karim, A.; Conant, T.; Datye, A. *J. Catal.* **2006**, *243*, 420–427.
(39) Conant, T.; Karim, A. M.; Lebarbier, V.; Wang, Y.; Girgsdies, F.; Schlogl, R.; Datye, A. *J. Catal.* **2008**, *257*, 64–70.
(40) Hyman, M. P.; Lebarbier, V. M.; Wang, Y.; Datye, A. K.; Vohs, J. A. *J. Phys. Chem. C* **2009**, *113*, 7251–7259.
(41) Lee, J. K.; Ko, J. B.; Kim, D. H. *Appl. Catal., A* **2004**, *278*, 25–35.
(42) Turco, M.; Bagnasco, G.; Costantino, U.; Marmottini, F.; Montanari, T.; Ramis, G.; Busca, G. *J. Catal.* **2004**, *228*, 56–65.
(43) Mastalir, A.; Frank, B.; Szizybalski, A.; Soerijanto, H.; Deshpande, A.; Niederberger, M.; Schomacker, R.; Schlogl, R.; Ressler, T. *J. Catal.* **2005**, *230*, 464–475.
(44) Frank, B.; Jentoft, F. C.; Soerijanto, H.; Krohnert, J.; Schlogl, R.; Schomacker, R. *J. Catal.* **2007**, *246*, 177–192.
(45) Greeley, J.; Mavrikakis, M. *J. Catal.* **2002**, *208*, 291–300.
(46) Mei, D. H.; Xu, L. J.; Henkelman, G. *J. Phys. Chem. C* **2009**, *113*, 4522–4537.
(47) Desai, S. K.; Neurock, M.; Kourtakis, K. *J. Phys. Chem. B* **2002**, *106*, 2559–2568.
(48) Greeley, J.; Mavrikakis, M. *J. Am. Chem. Soc.* **2004**, *126*, 3910–3919.
(49) Chen, Z. X.; Neyman, K. M.; Lim, K. H.; Rosch, N. *Langmuir* **2004**, *20*, 8068–8077.
(50) Jiang, R. B.; Guo, W. Y.; Li, M.; Fu, D. L.; Shan, H. H. *J. Phys. Chem. C* **2009**, *113*, 4188–4197.
(51) Bo, J. Y.; Zhang, S. R.; Lim, K. H. *Catal. Lett.* **2009**, *129*, 444–448.
(52) Kresse, G.; Furthmuller, J. *Phys. Rev. B* **1996**, *54*, 11169–11186.
(53) Kresse, G.; Furthmuller, J. *Comput. Mater. Sci.* **1996**, *6*, 15–50.
(54) Blochl, P. E. *Phys. Rev. B* **1994**, *50*, 17953–17979.
(55) Perdew, J. P.; Burke, K.; Ernzerhof, M. *Phys. Rev. Lett.* **1996**, *77*, 3865–3868.
(56) Perdew, J. P.; Wang, Y. *Phys. Rev. B* **1992**, *45*, 13244–13249.
(57) Monkhorst, H. J.; Pack, J. D. *Phys. Rev. B* **1976**, *13*, 5188–5192.
(58) Methfessel, M.; Paxton, A. T. *Phys. Rev. B* **1989**, *40*, 3616–3621.
(59) Henkelman, G.; Uberuaga, B. P.; Jonsson, H. *J. Chem. Phys.* **2000**, *113*, 9901–9904.
(60) Henkelman, G.; Jonsson, H. *J. Chem. Phys.* **2000**, *113*, 9978–9985.
(61) Carrasco, J.; Michaelides, A.; Scheffler, M. *J. Chem. Phys.* **2009**, *130*, 184707.
(62) Gomes, J. R. B.; Gomes, J. *Surf. Sci.* **2001**, *471*, 59–70.
(63) Mei, D. H.; Xu, L.; Henkelman, G. *J. Catal.* **2008**, *258*, 44–51.
(64) Phatak, A. A.; Delgass, W. N.; Ribeiro, F. H.; Schneider, W. F. *J. Phys. Chem. C* **2009**, *113*, 7269–7276.
(65) Xu, L. J.; Mei, D. H.; Henkelman, G. *J. Chem. Phys.* **2009**, *131*, 244520.
(66) Mehmood, F.; Greeley, J.; Curtiss, L. A. *J. Phys. Chem. C* **2009**, *113*, 21789–21796.
(67) Lim, K. H.; Chen, Z. X.; Neyman, K. M.; Rosch, N. *J. Phys. Chem. B* **2006**, *110*, 14890–14897.
(68) Nishimura, H.; Yatsu, T.; Fujitani, T.; Uchijima, T.; Nakamura, J. *J. Mol. Catal. A* **2000**, *155*, 3–11.
(69) Schumacher, N.; Boisen, A.; Dahl, S.; Gokhale, A. A.; Kandoi, S.; Grabow, L. C.; Dumesic, J. A.; Mavrikakis, M.; Chorkendorff, I. *J. Catal.* **2005**, *229*, 265–275.
(70) Brønsted, J. N. *Chem. Rev.* **1928**, *5*, 231–338.
(71) Evans, M. G.; Polanyi, M. *Trans. Faraday Soc.* **1938**, *34*, 0011−0023.
(72) Nørskov, J. K.; Bligaard, T.; Logadottir, A.; Bahn, S.; Hansen, L. B.; Bollinger, M.; Bengaard, H.; Hammer, B.; Sljivancanin, Z.; Mavrikakis, M.; Xu, Y.; Dahl, S.; Jacobsen, C. J. H. *J. Catal.* **2002**, *209*, 275–278.
(73) Michaelides, A.; Liu, Z. P.; Zhang, C. J.; Alavi, A.; King, D. A.; Hu, P. *J. Am. Chem. Soc.* **2003**, *125*, 3704–3705.
(74) Pallassana, V.; Neurock, M. *J. Catal.* **2000**, *191*, 301–317.
(75) Logadottir, A.; Rod, T. H.; Nørskov, J. K.; Hammer, B.; Dahl, S.; Jacobsen, C. J. H. *J. Catal.* **2001**, *197*, 229–231.
(76) Loffreda, D.; Delbecq, F.; Vigne, F.; Sautet, P. *Angew. Chem., Int. Ed.* **2009**, *48*, 8978–8980.
(77) Alcala, R.; Mavrikakis, M.; Dumesic, J. A. *J. Catal.* **2003**, *218*, 178–190.

JP107678D